Breast Cancer - Targets and Therapy

Dovepress
open access to scientific and medical research

Open Access Full Text Article

ORIGINAL RESEARCH

SR-B1-targeted nanodelivery of anti-cancer agents: a promising new approach to treat triple-negative breast cancer

Rebecca Johnson[1]
Nirupama Sabnis[2]
Xiangle Sun[1]
Ruhani Ahluwalia[3]
Andras G Lacko[2,4]

[1]Institute of Molecular Medicine, [2]Institute for Cardiovascular and Metabolic Diseases, University of North Texas Health Science Center, [3]Harmony School of Innovation, [4]Department of Pediatrics, University of North Texas Health Science Center, Fort Worth, TX, USA

Abstract: Patients with triple-negative breast cancer (TNBC) have a considerably less favorable prognosis than those with hormone-positive breast cancers. TNBC patients do not respond to current endocrine treatment and have a 5-year survival prognosis of <30%. The research presented here is intended to fill a void toward the much needed development of improved treatment strategies for metastatic TNBC. The overall goal of this research was to evaluate the effectiveness of reconstituted high-density lipoprotein (rHDL) nanoparticles (NPs) as delivery agents for anti-TNBC drugs. Using lapatinib and valrubicin as components of the rHDL/drug complexes resulted in a significantly better performance of the NP-transported drugs compared with their free (unencapsulated) counterparts. The enhancement of the therapeutic effect and the protection of normal cells (cardiomyocytes) achieved via the rHDL NPs were likely due to the overexpression of the high-density lipoprotein (HDL) (scavenger receptor class B type 1 [SR-B1]) receptor by the TNBC cells.

Keywords: breast cancer, TNBC, rHDL nanoparticles, SR-B1 receptors, targeted drug delivery, lapatinib, valrubicin

Video abstract

Point your SmartPhone at the code above. If you have a QR code reader the video abstract will appear. Or use: http://youtu.be/uMSaPk4D8os

Correspondence: Andras G Lacko
Institute of Cardiovascular and Metabolic Diseases, University of North Texas Health Science Center, 3500 Camp Bowie Blvd, Fort Worth, TX 76107, USA
Email andras.lacko@unthsc.edu

Introduction

Cancer continues to be a major health challenge causing the second highest number of fatalities in the US. Breast cancer (BC) cases may be classified into three major groups, estrogen receptor positive (ER^+), estrogen receptor negative (ER^-), and human epidermal growth factor receptor 2 positive ($HER2^+$) – either ER- or ER^+.[1,2] Those BC tumors that do not express any of these molecular biomarkers are termed triple-negative breast cancer (TNBC), a high-grade, highly proliferative, metastatic disease that does not respond to established endocrine therapy.[3] Although 15%–20% of all BC cases are of the TNBC subtype, this form of the disease accounts for a disproportionately high number of cancer deaths.[3,4] TNBC is frequently associated with a poor prognosis, primarily as the result of recurrence and visceral and brain metastases within the first 5 years of the initial diagnosis.[5–8] Although TNBC patients tend to initially respond to chemotherapy, their overall response to treatment is poor in comparison to HER2-positive patients.[9] The preferred treatment for women with early-stage or locally advanced TNBC is taxane based or anthracycline regimens because these agents are associated with high rates of complete response.[10] Despite their effectiveness against various types of tumors, the use of anthracyclines in chemotherapy is limited due to their intense cardiotoxicity.[11] For patients with metastatic disease, sequential single agents or combination therapies have been used; however, no single approach has so

far resulted in improved survival.[12] Developing multidrug resistance (MDR) by TNBC tumors has been one of the major reasons for unsuccessful chemotherapy.[13,14]

As an alternative to traditional therapy, nanoparticles (NPs) provide an effective mechanism for drug delivery to malignant cells and tumors by limiting off-target effects that damage healthy tissues.[15] NPs are anticipated to increase the therapeutic index of anti-cancer agents by prolonging circulating half-life, increasing drug accumulation in the tumor, and reducing the risk of off-target effects.[15] In addition to the above-listed advantages, NPs have been found to be highly effective as drug delivery vehicles by enhancing the efficacy of several drugs via active targeting and thus allowing the drugs to escape efflux pumps associated with drug resistance.[16,17]

Our laboratory has developed reconstituted high-density lipoprotein (rHDL) NPs for the purpose of improved drug delivery[18–21] to malignant cells and tumors.[18–22] High-density lipoproteins (HDLs) are endogenous cholesterol transporters. Their physicochemical properties and targeted delivery of their core components (including drugs) make them ideal transporters of anti-cancer agents.[23] The advantages of using rHDL NPs over most of the other drug delivery systems include their small size (>20 nm diameter), long circulation time, biocompatibility,[23] absence of immunogenic response, and their capability for tumor-selective delivery of the drug payload. This drug delivery strategy also seems superior to liposomal approaches because of the much smaller size of rHDL NPs and the scavenger receptor class B type 1 (SR-B1) receptor-mediated, tumor-selective delivery of their payload.[22]

It has been hypothesized that because cancer cells proliferate faster than normal cells, they may have a higher need for cholesterol than normal cells.[24] Earlier studies, in fact, revealed that cancer cells show enhanced proliferation in the presence of added HDL.[25] One way cancer cells may acquire the excess cholesterol needed for growth is by the overexpression of the HDL receptor or SR-B1.[26,27] Most cancer cells studied have been reported to overexpress the SR-B1 protein.[22,28] Recently, Yuan et al showed that 54% of malignant breast tumors had a high expression of the SR-B1 receptor. The great majority of the SR-B1-overexpressing tumor samples were obtained from TNBC patients.[29] Yuan et al[29] also developed a prediction algorithm that indicated a poorer outcome for BC patients whose tumors showed a high expression of the SR-B1 receptor. Using MDA-MB-231 TNBC cells, Danilo et al[26] found that migration can be induced by the addition of HDL3 to the culture medium. The studies of Danilo et al also revealed that these effects could be attenuated via the knockdown of SR-B1. These data suggest that SR-B1 is an important factor in malignancy as it promotes the survival and metastatic activity of cancer cells and tumors, including those associated with BC.

The present study was aimed to evaluate the use of rHDL-mediated drug delivery that takes advantage of the SR-B1 gateway to TNBC cells and tumors.[30] This "Trojan Horse" strategy[18] has proven effective for a number of malignant cells;[18–21] therefore, it is anticipated to provide a foundation for the development of novel therapeutic approaches for TNBC.

Materials and methods

Cell culture and chemicals

MDA-MB-231 (TNBC) and H9C2 (cardiomyocyte cells; ATCC, Manassas, VA, USA) were grown in 75 cm^2 flasks containing Dulbecco's Modified Eagle Medium (DMEM) high-glucose media with phenol red (Thermo Fisher Scientific, Waltham, MA, USA) supplemented with 10% fetal bovine serum (FBS; HyClone, Logan, UT, USA) incubated at 37°C in a humidified incubator at 5% CO2. Stock solutions of valrubicin (China Kouting Group Ltd., Shenzhen, China) at 50 mg/mL and lapatinib at 25 mg/mL (Selleck Chemicals, Houston, TX, USA) were prepared in dimethyl sulfoxide (DMSO) and kept at −20°C.

Preparation of drug containing rHDL NPs

A mixture of egg yolk phosphatidylcholine (PC; 7.5 mg/mL), free cholesterol (FC; 0.175 mg/mL), and cholesteryl oleate (CE; 0.075 mg/mL) was pipetted into a glass vial from respective stocks in chloroform, and the chloroform was subsequently evaporated under nitrogen gas to form a thin film inside the vial. The drugs (lapatinib or valrubicin) were added at a concentration of 1 mg/mL to the lipids, followed by 30 µL DMSO and apo A-I (2.5 mg/mL; MCLAB, San Francisco, CA, USA), and mixed thoroughly by vortexing. To this mixture, 7 mg/mL sodium cholate was added (from a stock of 100 mg/mL), and the preparation was made up to a final volume of 1 mL by adding a buffer solution (10 mM Tris, 0.1 M KCl, 1 mM EDTA, pH 8.0). The sample was then frozen at −80°C overnight. Subsequently, the NP preparation was lyophilized, redissolved in water, and dialyzed against 2 L of phosphate-buffered saline (PBS) for 48 hours. After dialysis, the preparations were centrifuged at 3300 ×*g* for 1 minute, and the supernatant was collected. The NP preparation was then syringe filtered through a 0.45 µm pore filter (EMD Millipore, Billerica, MA, USA). The preparations were kept at 4°C until used.

Determination of drug entrapment efficiency (DEE)

Entrapment efficiency was determined as reported previously.[20] Briefly, entrapment efficiency was determined by measuring the amount of initial (before dialysis) and final (after filtration) drug concentrations. In a 96-well plate, series of dilutions of rHDL–valrubicin NPs and rHDL–lapatinib NPs were prepared using PBS with 1% triton, and the absorbance was read at 490 nm. rHDL–lapatinib NPs were mixed with PBS in the presence of 1% Triton X-100, and the absorbance was read at 490 or 362 nm for valrubicin and lapatinib, respectively. The respective drug concentrations were extrapolated using a standard graph for each drug.

DEE = {drug concentration after dialysis and filtration/ drug concentration before dialysis}×100. (1)

Preparation of rHDL/H-cholesteryl oleate complex

A mixture of egg yolk PC in chloroform with labeled cholesterol oleate and CE was prepared with a molar ratio of apo A-1:FC:CE:PC = 1:5:1.3:1.15. Chloroform was evaporated from PC, CE, and CE under nitrogen gas to a thin film and rehydrated in 60 μL DMSO for a 2 mL preparation. To this mix, apo A-I (2.5 mg/mL) and 140 μL sodium cholate (from a stock of 100 mM) were added with sodium cholate buffer (10 mM Tris, 0.1 M KCl, and 1 mM EDTA, pH 8.0) to make a volume of 2 mL. The cholate/lipid/protein mixture was then frozen in the −80°C freezer overnight. Preparations were then dialyzed for 48 hours against 2 L of PBS, with three buffer changes during the first 6 hours. After dialysis, the preparations were centrifuged at 3300 ×*g* for 1 minute and kept at 4°C until used.

Determination of chemical composition of the rHDL NPs

Pierce BCA protein assay kit (Thermo Fisher Scientific) was used to determine protein concentration. The amounts of cholesterol and phospholipid contained in the NPs were determined by respective enzymatic reagent kits (cholesterol E and phospholipid C; Wako Chemicals, Richmond, VA, USA) using microtiter plate assays as per manufacturer's suggestions. All assays were read on the PowerWave 340 microplate reader (BioTek Instruments, Winooski, VT, USA) at the appropriate wavelength.

Particle diameter measurements

rHDL/valrubicin and rHDL/lapatinib NP size estimations were performed using dynamic light scattering (DLS) carried out using a Nanotrac system (Microtrac Inc., Montgomeryville, PA, USA) as per manufacturer's instructions. rHDL/lapatinib NP size was also established by transmission electron microscopy (TEM). Following dialysis in a volatile buffer (0.125 M ammonium acetate, 2.6 mM ammonium carbonate, 0.26 mM EDTA, pH 7.4), the isolated rHDL samples were negatively stained with 2% sodium phosphotungstate, pH 7.2, and placed on formvar/carbon-coated 200 mesh nickel grid support films (Ted Pella Inc., Redding, CA, USA) as previously described.19 The particles were visualized using a magnification of 50,000 on a Zeiss 910 transmission electron microscope (Carl Zeiss, Thornwood, NY, USA).

Determination of IC_{50} by cytotoxicity assay

The impact of valrubicin and lapatinib on the viability of normal and cancer cells was estimated using the cell counting kit-8 (CCK-8; Dojindo Molecular Technologies, Gathesburg, MD, USA). H9C2 and MDA-MB-231 cells (6000 cells/well) were seeded into 96-well microtiter plates and incubated at 37°C in 5% CO2 atmosphere overnight. Free drug formulations were diluted in serum-free media to yield the concentrations (2–8 μM). After incubation, 10 μL of a tetrazolium salt, 2-(2-methoxy-4-nitrophenyl)-3-(4-nitrophenyl)-5-(2,4-disulfophenyl)-2H-tetrazolium (WST-8; monosodium salt), stock solution was added to all wells. The reagent was thoroughly mixed. After a 3-hour incubation period, the absorbance at 450 nm was read using a PowerWave 340 microplate reader. There were four replicates for each concentration. Each experiment was repeated at least three times.

Flow cytometry analysis of SR-B1 expression

A total of 750,000 cells were plated and cultured in a 100 mm Petri dish. Cells were collected and washed with 1× PBS twice, followed by a wash with staining buffer (1× PBS, 2% FBS, 0.1% sodium azide). Next, cells were seeded in a 96 round-bottom plate at 1×10^6 cells/well. Cells were blocked with anti-goat serum for 30 minutes at room temperature and then treated with 1:50 dilution of SR-B1 rabbit-anti-human monoclonal antibody (Abcam, Cambridge, MA, USA) in staining buffer for 30 minutes at room temperature. Cells were then washed in staining buffer for two times, followed by incubation with the secondary goat anti-rabbit Alexa Fluor 488-conjugated antibody at 1:2000 dilution for 30 minutes in the dark. Cells were pelleted and washed in staining buffer. Cells were acquired using the Cytomics FC 500 Cytometer and analyzed by CXP2.1 software (Beckman Coulter, Brea, CA, USA).

Confocal microscopy

MDA-MB-231 cells (7.5 × 104/well) were seeded onto poly-lysine-coated 12 mm coverslips (Corning Inc., Corning, NY, USA) in a six-well plate (Thermo Fisher Scientific) and incubated overnight at 37°C in an atmosphere of 5% CO_2. Cells were pretreated with 0.05 mg/mL of the block lipid transporter-1 (BLT-1; Sigma-Aldrich, St. Louis, MO, USA) or SR-B1 antibody (1:50 dilution) for 30 minutes. After pretreatment, the cells were treated with rHDL–valrubicin (8 μM) or free valrubicin at 8 μM concentration and incubated at 37°C with serum-free media for 3 hours. Cells were then washed three times with PBS containing 1% FBS. The coverslip (with the attached MDA-MB-231 cells) was removed from the six-well plate and mounted on microscope slides with 4,6-Diamidino-2-phenylindole, dihydrochloride (DAPI) antifade mounting serum (Molecular Probes, Eugene, OR, USA). The Zeiss LSM 510 microscope was used to obtain the confocal image of the cells at 40× magnification, at excitation/emission wavelengths of 488/518 nm for SR-B1, 488/561 nm for valrubicin, 405/461 nm for DAPI, and 650/668 nm for actin phalloidin.

Statistical analysis

All experimental data were obtained by calculating the mean value derived from five independent measurements. *p*-values were calculated at a 95% confidence interval and were considered statistically significant when <0.05. Differences in cell viability IC_{50} values were evaluated using the GraphPad Prism software (GraphPad Software Inc., La Jolla, CA, USA). The unpaired two-tailed Student's *t*-test was used to determine the significance of IC_{50} values between cell viability tests. Cell survival data were expressed as mean ± standard deviation. The paired Student's *t*-test was used to assess the difference in the radioactivity uptake by MBA study for assessing SR-B1 functionality. ImageJ software (Wayne Rasband, National Institutes of Health, Bethesda, MD, USA) was used to determine the fluorescence intensity of the confocal images. Fluorescence intensity was displayed as corrected total cell fluorescence (CTCF). The Student's *t*-test was used to compare the differences in fluorescence intensity in valrubicin–rHDL-treated TNBC cells vs free valrubicin treatment.

Results

Characterization of the valrubicin containing rHDL NPs

Valrubicin was incorporated into rHDL NPs using the procedure described earlier. The overall chemical composition of the rHDL–valrubicin NPs showed that the percentage of protein, phospholipid, cholesterol, and drug was 28.36%, 60.77%, 1.14%, and 9.72%, respectively (Table 1). The percentage chemical composition of these particles resembled that of native circulating HDL.[20] Data from DLS demonstrated that the formulation was reasonably homogeneous with the majority of the NPs showing an average diameter of 48.1 ± 6.1 nm (Figure 1A). These observations confirmed earlier findings regarding the size of the NPs[20] and were observed to be within the acceptable range for NPs to penetrate the tumor microenvironment.[31] The analysis of surface properties of rHDL–valrubicin NPs exhibited zeta potential of −6.43 ± 2.6 (Table 1).

Characterization of lapatinib containing rHDL NPs

The chemical composition of the lapatinib containing rHDL NPs is shown in Table 1 and Figure 1A. The NP components were determined by respective analyses as described in the "Materials and methods" section. The relative drug incorporation (19% for lapatinib) is one of the highest observed in our experience with several drug payloads.[19–21] The lapatinib–rHDL NPs were found to have a mean diameter of 34.8 ± 3.6 nm, assessed via DLS (Figure 1B), and a zeta potential of −8.8 ± 2.6 mV. Not surprisingly, the molecular diameter of the lapatinib-containing rHDL NPs was found to be considerably smaller (<20 nm; Figure 1C) when examined by TEM compared to the value yielded via DLS measurements (Figure 1B). We have consistently observed this trend with our rHDL NPs.

Assessment of the cytotoxicity of valrubicin and lapatinib formulations

To determine the effectiveness of valrubicin and lapatinib as free drugs vs drugs containing rHDL NPs, cell viability

Table 1 Chemical composition of the lapatinib containing rHDL NPs

rHDL/valrubicin and rHDL/lapatinib NP components, mg (%)					Zeta potential
NPs	**Protein**	**Phospholipid**	**Cholesterol**	**Drug**	
rHDL–lapatinib	5.88 (25)	12.4 (52)	0.8 (4)	4.6 (19)	−8.8 ± 2.6
rHDL–valrubicin	2.1 (28.36)	4.5 (60.77)	0.085 (1.14)	0.72 (9.72)	−6.43 ± 0.6

Abbreviations: rHDL, reconstituted high-density lipoprotein; NP, nanoparticle.

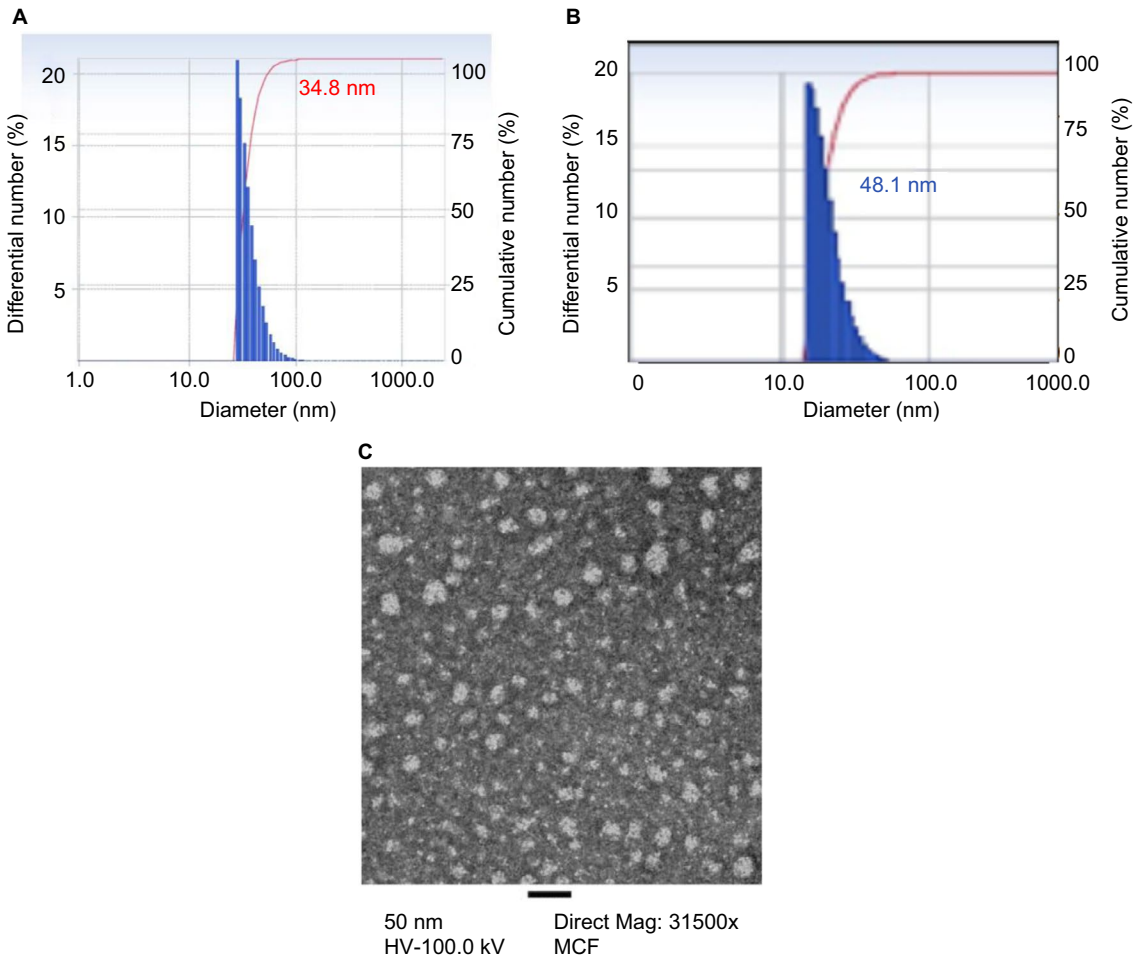

Figure 1 Particle size measurement by DLS and TEM.
Note: Particle diameter assessment for (**A**) valrubicin–rHDL NPs via DLS, (**B**) lapatinib–rHDL NPs via DLS, and (**C**) lapatinib–rHDL NPs via TEM.
Abbreviations: rHDL, reconstituted high-density lipoprotein; NP, nanoparticle; DLS, dynamic light scattering; TEM, transmission electron microscopy.

assays were performed. Because anthracyclines are known to be cardiotoxic, the impact of the valrubicin formulations on cardiomyocytes (H9C2) was also assessed. Untreated cells were used as controls. The cell viability was determined over a 72-hour period using a CCK-8 kit as described in the "Materials and methods" section. The results of the cell viability assays for the free (unencapsulated) and the rHDL–valrubicin-treated TNBC (MB-MDA23) cells are shown in Figure 2A. The regression lines (Figure 2A) and the calculated IC_{50} values (Table 2) indicate that the rHDL/valrubicin formulation is more toxic toward TNBC cells than the free drug. Accordingly, the IC_{50} value for rHDL–valrubicin vs valrubicin was 2.3 ± 0.14 μM and 3.45 ± 0.19 μM, respectively. Similar assays performed with the H9C2 (cardiomyocyte) cell line (Figure 3A) gave rise to an exactly opposite trend (Table 2). Here, the free drug was considerably more effective in killing the cells (IC_{50} = 4.39 ± 0.39 μM) than the rHDL–valrubicin formulation (IC_{50}=7.53 ± 0.10 μM).

The broadening of the therapeutic window due to the incorporation of valrubicin into rHDL NPs was calculated using the formula shown as follows:

$$\frac{\text{Valrubicin } IC_{50} \text{ against MB-MDA231 cells}}{\text{rHDL} - \text{valrubicin } IC_{50} \text{ against MB-MDA231 cells}} \div \frac{\text{Valrubicin } IC_{50} \text{ against H9C2 cells}}{\text{rHDL} - \text{valrubicin } IC_{50} \text{ against H9C2 cells}} \quad (2)$$

This formula yields the following relationship:

$$\frac{3.45}{2.30} \div \frac{4.67}{7.63} = \frac{1.50}{0.61} = 2.48 \quad (3)$$

Accordingly, the therapeutic enhancement of valrubicin against TNBC cells resulting from the incorporation of the drug into rHDL NPs was ~2.5 fold. These findings indicate potential benefits for TNBC chemotherapy by limiting or avoiding off-target toxicity of the anti-cancer agent due to formulating it with rHDL.

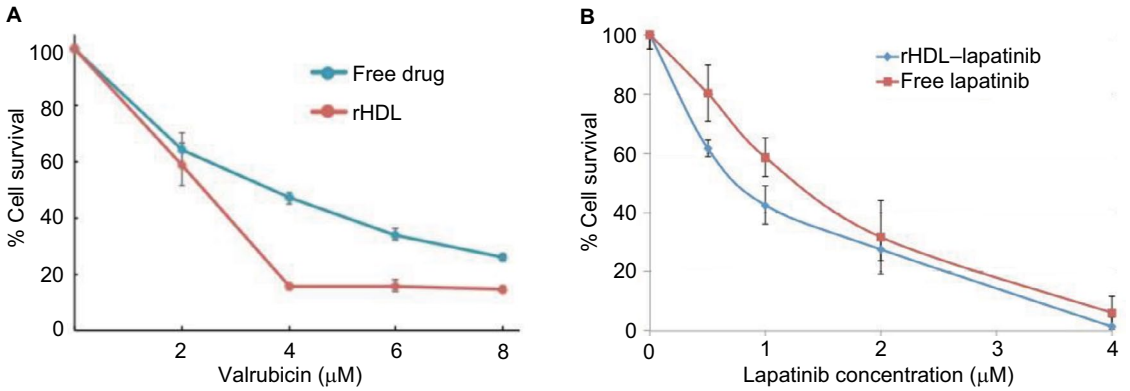

Figure 2 Assessment of (**A**) the impact of free valrubicin vs valrubicin incorporated into rHDL NPs on MDA-MB-231 (TNBC) cells and (**B**) cytotoxicity of free lapatinib vs rHDL–lapatinib against TNBC cells.
Abbreviations: rHDL, reconstituted high-density lipoprotein; NP, nanoparticle; TNBC, triple-negative breast cancer.

Table 2 Cytotoxicity of valrubicin vs rHDL–valrubicin against TNBC cells (MB-MDA231) and cardiomyocytes (H9C2)

Cell line	IC_{50} rHDL/drug (μM)	IC_{50} free drug (μM)
H9C2	7.53 ± 0.01	4.67 ± 0.39
MDA-MB-231	2.29 ± 0.39	3.47 ± 0.06

Note: Data presented as mean ± standard deviation.
Abbreviations: rHDL, reconstituted high-density lipoprotein; TNBC, triple-negative breast cancer.

Cytotoxicity of lapatinib against TNBC (MDA-MB-231) cells

The cytotoxicity studies involving lapatinib were conducted in a manner similar to those with valrubicin (Figure 2). The data shown in Figure 2B indicate that the rHDL–lapatinib NPs are more effective against TNBC cells (IC_{50} = 0.78 ± 0.04 μM) than the free drug (IC_{50} = 1.40 ± 0.59 μM). When the rHDL–lapatinib formulation was used against H9C2 cells, the free lapatinib had IC_{50} values that were less than half (9.68 ± 3.4) than those of rHDL–lapatinib (>20 nM) as shown in Table 3. Overall, the rHDL–lapatanib formulation had a protective effect against cardiomyocytes as indicated in Figure 3B. When the abovementioned formula (2) was applied to calculate the expanding of the therapeutic window via formulating lapatinib with rHDL NPs, the therapeutic enhancement was estimated to be approximately fourfold for rHDL–lapatinib vs free lapatinib.

Role of the SR-B1 receptor in delivering anti-cancer agents to TNBC cells

Northern blot analyses of cancer cell lines revealed that the TNBC cells (MDA-MB-231) showed a high expression of the SR-B1 receptor.[22] However, because mRNA levels do not always correlate strictly with expressed protein levels and protein function, therefore, flow cytometry was used to determine the SR-B1 protein expression levels in TNBC and cells (MDA-MB-231) and a cardiomyocyte cell line (H9C2; Figure 4). In Figure 4, the dotted line represents the level of autofluorescence that the cells emit naturally, while the solid line represents the mean fluorescence intensity, indicating the level of SR-B1 protein expression by the respective cells. The amount of SR-B1 protein can be estimated by assessing the shift in fluorescence intensity (to the right). In Figure 4, the cardiomyocytes show almost no shift in fluorescence

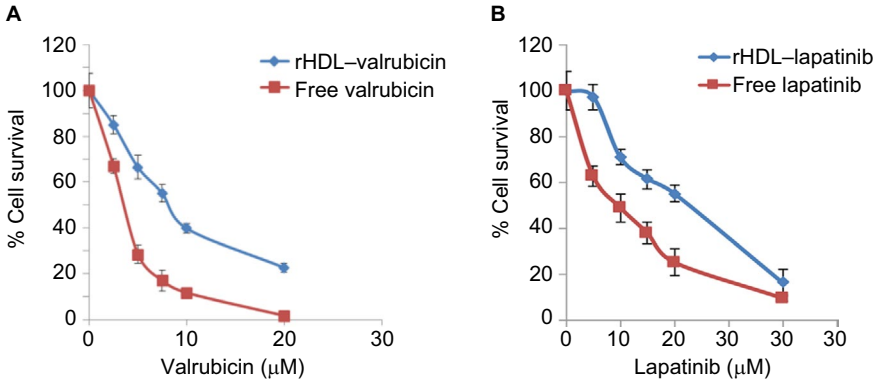

Figure 3 Assessment of the impact of (**A**) free valrubicin vs valrubicin incorporated into rHDL NPs on H9C2 (cardiomyocyte) cells and (**B**) free lapatinib vs lapatinib incorporated into rHDL NPs on H9C2 (cardiomyocyte) cells.
Abbreviations: rHDL, reconstituted high-density lipoprotein; NP, nanoparticle.

Table 3 Cytotoxicity of lapatinib vs. rHDL–lapatinib against TNBC cells (MDA-MB-231) and cardiomyocytes (H9C2)

Cell line	IC_{50} rHDL/drug (μM)	IC_{50} free drug (μM)
H9C2	>20	9.68 ± 3.40
MDA-MB-231	0.75 ± 0.39	1.4 ± 0.06

Note: Data presented as mean ± standard deviation.
Abbreviations: rHDL, reconstituted high-density lipoprotein; TNBC, triple-negative breast cancer.

intensity, while the MDA-MB-231 cell line does show a significantly higher shift ($t = 17.26$; $p < 0.01$), indicating that the TNBC cell line, unlike the cardiomyocytes, robustly expresses the SR-B1 protein.

To further validate the role of the SR-B1 as a gateway for anti-cancer drug delivery to TNBC cells, the functional capabilities of this receptor were assessed. 3H-cholesteryl oleate was incorporated into rHDL NPs, as described in the "Materials and methods" section. MDA-MB-231 cells were incubated with the radioactively labeled rHDL NPs in the presence and absence of an SR-B1 inhibitor (BLT-1). The findings show a nearly complete inhibition of the cholesteryl oleate uptake by the MDA–MB-231 cells in the presence of the highest concentration of BLT-1, apparently blocking the function of the SR-B1 receptor (Figure 5).

Confocal microscopy studies for the validation of the SR-B1 drug delivery model

To investigate the rHDL drug delivery mechanism, further confocal images were taken of rHDL–valrubicin-treated MDA-MB-231 cells vs free drug-treated cells. Before taking confocal images of treated MDA-MB-231 cells, a confocal image of the untreated cell line was taken as a control (data not shown). Here, the cells were stained for F-actin (magenta). The image demonstrates the epithelial-to-mesenchymal transition (EMT), a spindle-like shape of the cells. An image of MDA-MB-231 cells after being treated with the free drug (valrubicin) and the rHDL–valrubicin preparation (8 μM) for a 3-hour period is depicted in Figure 6. The fluorescent intensity of the cells was measured using the ImageJ software. The fluorescence intensity is a measure of the amount of drug that has entered the cell. There was a significantly higher fluorescence intensity observed in the rHDL-treated cells than in the cells treated with the free drug ($t = 3.45$, $p < 0.05$), indicating that significantly more drug accumulated within the cell when treated with rHDL–valrubicin vs those treated with the free drug.

To investigate that the rHDL NPs are specifically interacting with the SR-B1 receptor, a chemical inhibitor of the receptor, BLT-1, was used. Subsequently, the cells were also treated with rHDL–valrubicin (Figure 7) or the free drug (Figure 8) at 8 μM concentration. After 3 hours, the cells were washed, and confocal images were taken. The data in Figure 7 show that the capacity of the rHDL–valrubicin-treated cells for drug uptake was significantly reduced in the presence of the BLT-1 inhibitor ($p < 0.01$). Figure 8 depicts the inhibition-free valrubicin uptake by MDA-MB-231 cells in the presence of the BLT-1 inhibitor. The data show (Figure 8) that the BLT-1 (SR-B1) inhibitor had little or no effect on the uptake of free (unencapsulated) valrubicin by the MDA-MB-231 cells, as indicated by the absence of a significant decrease in fluorescence intensity. The data in Figure 9 provide further support for the receptor-mediated (SR-B1) mechanism of

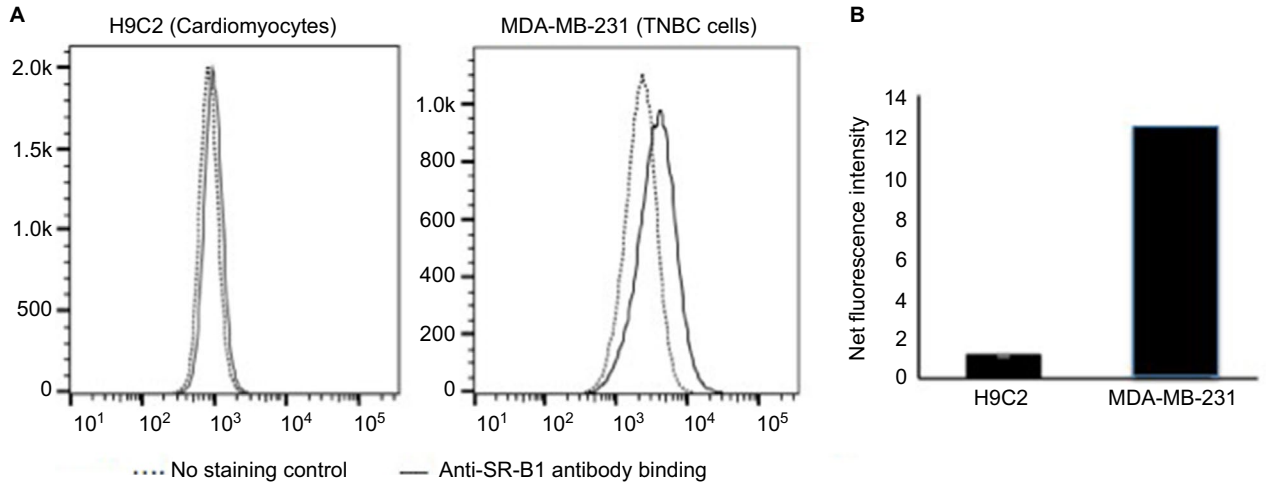

Figure 4 Flow cytometry analysis of SR-B1 expression in malignant vs normal cells.
Notes: (**A**) Mean fluorescence intensity. (**B**) Quantitative comparison of the estimates of the SR-B1 expression by the respective cell lines.
Abbreviations: SR-B1, scavenger receptor class B type 1; TNBC, triple-negative breast cancer.

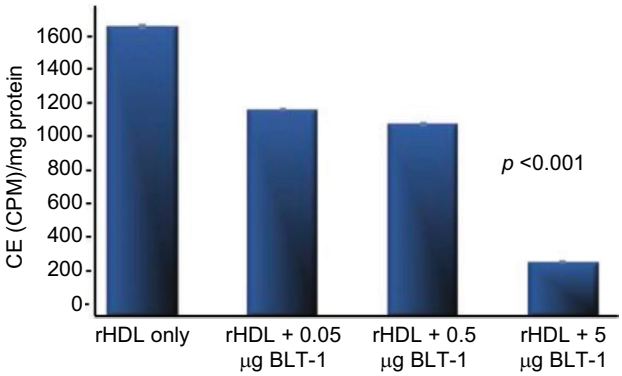

Figure 5 Radioactive CE uptake from rHDL in the presence of a chemical inhibitor BLT-1 by MDA-MB-231 cells (n = 4/dose).
Abbreviations: rHDL, reconstituted high-density lipoprotein; BLT-1, block lipid transporter-1; CE, cholesteryl oleate; CPM, radioactive counts per minute.

the valrubicin uptake from rHDL–valrubicin as the SR-B1 antibody appears to completely block the valrubicin uptake by the MDA-MB-231 cells. These results confirm our earlier findings[18–22] that the drug delivery via rHDL NPs is indeed facilitated by the SR-B1 receptor.

Discussion

While the current average 5-year survival rate for BC patients is 89.2%,[32] the 5-year survival prognosis for patients with metastatic TNBC is <30%.[5] This unusually low survival impacts African-American women disproportionately as ~50% of African American women with BC at the age of 40 years or younger present with the TNBC type.[33] Current

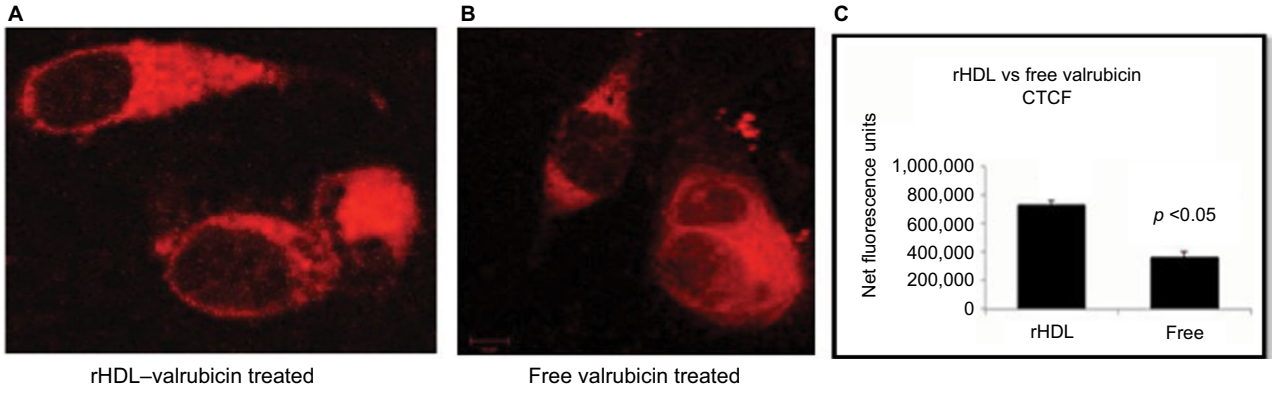

Figure 6 Confocal microscopey images of valrubicin treated MDA-MB-231 cells.
Notes: The images depict the amount of valrubicin that has entered the cell after a 3-hour period: (**A**) free valrubicin (8 μM) and (**B**) rHDL–valrubicin (8 μM). Magnification ×40. The accompanying bar graph (**C**) shows the CTCF (n = 3). The data show a significantly higher uptake by the rHDL–valrubicin-treated cells ($t = 3.45$; $p < 0.05$).
Abbreviations: rHDL, reconstituted high-density lipoprotein; CTCF, corrected total cell fluorescence.

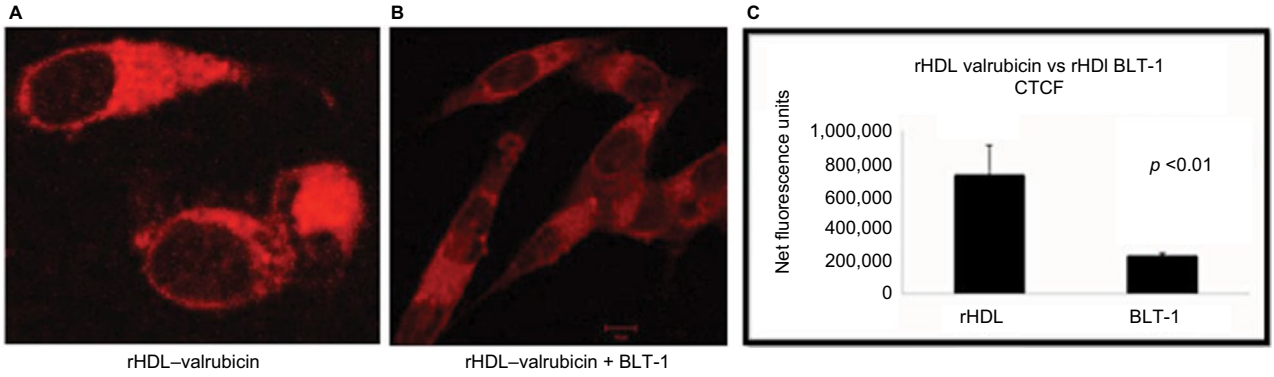

Figure 7 Confocal microscopy images of MDA-MB 231 treated with rHDL-valrubicin in presence of BLT-1.
Notes: (**A** and **B**) Confocal microscope images of valrubicin uptake by MDA-MB-231 cells from rHDL–valrubicin NPs in the presence of an SR-B1 inhibitor (BLT-1). MDA-MB-231 cells were treated with BLT-1 (0.5 mg/mL) and subsequently with rHDL–valrubicin (8 μM) for 3 hours. Magnification ×40. The accompanying bar graph (**C**) shows the CTCF (n = 3). The data show a significantly decrease valrubicin uptake by the BLT-1-treated cells ($p < 0.01$).
Abbreviations: rHDL, reconstituted high-density lipoprotein; NP, nanoparticle; SR-B1, scavenger receptor class B type 1; BLT-1, block lipid transporter-1; CTCF, corrected total cell fluorescence.

treatment options for TNBC are limited and often lead to inadequate response and low survival rates.[34] In addition, the chemotherapeutic agents currently in use present with substantial off-target effects therefore, detract from the potential benefits of therapy.[35,36] NPs have provided promising alternatives to traditional therapy by enhancing the therapeutic index and an improved antitumor effect.[18–22] The rHDL NPs loaded with chemotherapeutic agents appear to have highly desirable characteristics needed for improved TNBC chemotherapy.[15] These include the following:

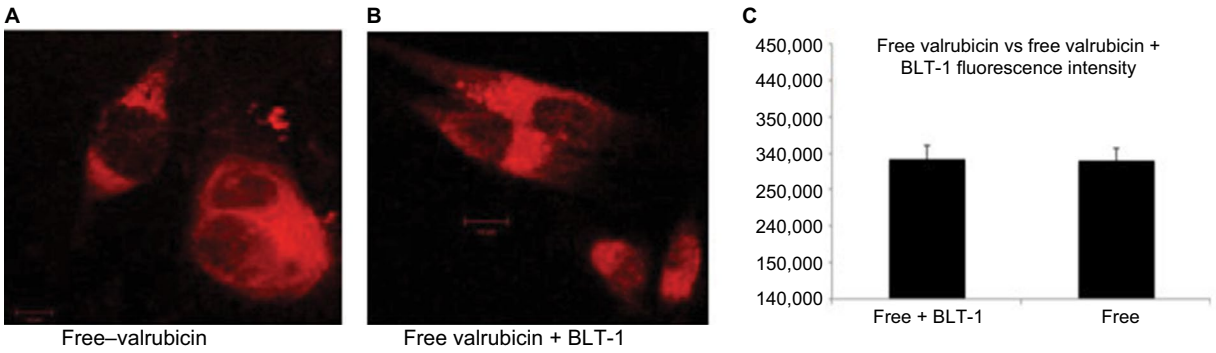

Figure 8 Confocal microscopy images of MDA-MB 231 treated with free valrubicin in presence of BLT-1.
Notes: (**A** and **B**) Confocal microscope images of BLT-1 and free valrubicin uptake by MDA-MB-231 cells in the presence of BLT-1 at 0.5 mg/mL. Magnification ×40. The accompanying bar graph (**C**) shows no significant decrease in valrubicin uptake by the BLT-1-treated cells.
Abbreviation: BLT-1, block lipid transporter-1.

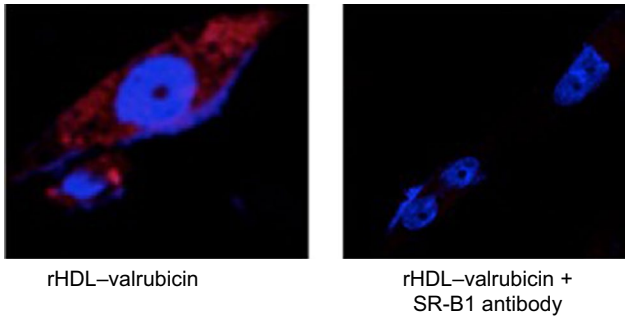

Figure 9 Confocal microscopey images (**A** and **B**) of rHDL–valrubicin uptake by MDA-MB-231 cells following pretreatment with an SR-B1 antibody. Magnification ×40.
Abbreviations: SR-B1, scavenger receptor class B type 1; rHDL, reconstituted high-density lipoprotein.

1. the relatively small size of the rHDL NPs could be a major therapeutic advantage vs conventional drug carriers (including liposomes) as smaller particles are anticipated to penetrate the tumor environment more successfully;[31]
2. extended circulation time, due to the ability to avoid the mononuclear phagocyte system that clears the most of the nanoparticulate foreign bodies from the blood; and
3. tumor-selective targeted drug delivery[18] (see in the following section).

The rHDL NPs loaded with chemotherapeutic agents thus appear to have highly desirable characteristics needed for improved TNBC chemotherapy.

During this study, two drugs (valrubicin and lapatinib) were evaluated regarding their potential contributions to TNBC therapy. These studies show that the rHDL NPs facilitate active targeting of both drugs via the SR-B1 receptor that is overexpressed by most cancer cells and tumors (including those involved with TNBC).[22] These studies have also shown that tumor-selective delivery of the anti-cancer drug payload of the rHDL NPs via the SR-B1 receptor is feasible as evidenced by the uptake of radioactive cholesteryl esters by TNBC cells (Figure 5) and confocal microscopy experiments (Figures 6–9).

Regarding the receptor-mediated drug delivery, the cytosolic targeting of anti-cancer agents[37] could be another major advantage of the rHDL transport system because rHDL NPs may have the ability to deliver their payload directly to the cytoplasm and thus avoid the drug resistance pump mechanisms located in the cell membrane. Taken together, these findings show that the MDA-MB31 cells acquire drugs from rHDL NPs via a targeted, receptor-mediated mechanism,[30] validating the proposed approach to serve as a potentially enhanced therapy for TNBC. The rHDL NPs are expected to resist opsonization and subsequent sequestering of the NPs by the reticuloendothelial system, one of the current barriers to effective chemotherapy.

At the same time, these particles showed protective effect against cardiomyocytes due to their limited SR-B1 expression. This observation suggests reduction or elimination of cardiac side effects when drugs are encapsulated in rHDL NPs during therapy.

Acknowledgment

This research was supported by the Cancer Prevention and Research Institute of Texas (DP150091); Wheels for Wellness, Fort Worth, TX, USA; and the Rutledge Foundation.

Disclosure

The authors report no conflicts of interest in this work.

References

1. World Health Organization. In: Stewart B, Wild C, editors. *World Cancer Report 2014*. 2014. Available from https://www.iarc.fr/en/media-centre/pr/2014/pdfs/pr224_E.pdf. Accessed December 12, 2014.
2. Miles D. Recent advances in systemic therapy. When HER2 is not the target: advances in treatment of HER2-negative metastatic breast cancer. *Breast Cancer Res*. 2009;11(4):208.

3. Rakha EA, Reis-Filho JS, Ellis IO. Basal-like breast cancer: a critical review. *J Clin Oncol*. 2008;26(15):2568–2581.
4. Cleator S, Heller W, Coombes RC. Triple-negative breast cancer: therapeutic options. *Lancet Oncol*. 2007;8(3):235–244.
5. Liedtke C, Mazouni C, Hess KR, et al. Response to neoadjuvant therapy and long-term survival in patients with triple-negative breast cancer. *J Clin Oncol*. 2008;26(8):1275–1281.
6. Bos PD, Zhang XH, Nadal C, et al. Genes that mediate breast cancer metastasis to the brain. *Nature*. 2009;459(7249):1005–1009.
7. Hudis CA, Gianni L. Triple-negative breast cancer: an unmet medical need. *Oncologist*. 2011;16(suppl 1):1–11.
8. Mancini P, Angeloni A, Risi E, Orsi C, Mezi S. Standard of care and promising new agents for triple negative metastatic breast cancer. *Cancers (Basel)*. 2014;6(4):187–223.
9. Lehmann BD, Bauer JA, Chen X, et al. Identification of human triple-negative breast cancer subtypes and preclinical models for selection of targeted therapies. *J Clin Invest*. 2011;121(7):2750–2767.
10. Schettini F, Giuliano M, De Placido S, Arpino G. Nab-paclitaxel for the treatment of triple-negative breast cancer: rationale, clinical data and future perspectives. *Cancer Treat Rev*. 2016;50:129–141.
11. Hagiwara H, Sunada Y. Mechanism of taxane neurotoxicity. *Breast Cancer*. 2004;11(1):82–85.
12. Zhang JF, Liu J, Wang Y, Zhang B. Novel therapeutic strategies for patients with triple-negative breast cancer. *Onco Targets Ther*. 2016;9:6519–6528.
13. Lee ES, Na K, Bae YH. Doxorubicin loaded pH-sensitive polymeric micelles for reversal of resistant MCF-7 tumor. *J Control Release*. 2005;103(2):405–418.
14. Patel NR, Rathi A, Mongayt D, Torchilin VP. Reversal of multidrug resistance by co-delivery of tariquidar (XR9576) and paclitaxel using long-circulating liposomes. *Int J Pharm*. 2011;416(1):296–299.
15. Johnson R, Sabnis N, McConathy WJ, Lacko AG. The potential role of nanotechnology in therapeutic approaches for triple negative breast cancer. *Pharmaceutics*. 2013;5(2):353–370.
16. Guo Y, He W, Yang S, Zhao D, Li Z, Luan Y. Co-delivery of docetaxel and verapamil by reduction-sensitive PEG-PLGA-SS-DTX conjugate micelles to reverse the multi-drug resistance of breast cancer. *Colloids Surf B Biointerfaces*. 2017;151:119–127.
17. Zhang Y, Leonard M, Shu Y, et al. Overcoming tamoxifen resistance of human breast cancer by targeted gene silencing using multifunctional prank nanoparticles. *ACS Nano*. 2017;11(1):335–346.
18. Lacko A, Nair M, Paranjape S, Mooberry L, McConathy W. Trojan horse meets magic bullet to spawn a novel, highly effective drug delivery model. *Chemotherapy*. 2006;52(4):171–173.
19. McConathy WJ, Nair M, Paranjape S, Mooberry L, Lacko AG. Evaluation of synthetic/reconstituted high density lipoproteins (rHDL) as delivery vehicles for paclitaxel. *Anticancer Drugs*. 2008;19(2):183–188.
20. Sabnis NA, Nair M, Israel M, McConathy WJ, Lacko AG. Enhanced solubility and functionality of valrubicin (AD-32) against cancer cells upon encapsulation into biocompatible nanoparticles. *Int J Nanomedicine*. 2012;7:975–983.
21. Sabnis N, Pratap S, Akopova I, Bowman WP, Lacko AG. Pre-clinical evaluation of rHDL encapsulated retinoid for the treatment of neuroblastoma. *Front Pediatr Oncol*. 2013;1:1–10.
22. Shahzad MM, Mangala LS, Han HD, et al. Targeted delivery of small interfering RNA using reconstituted high-density lipoprotein nanoparticles. *Neoplasia*. 2011;13(4):309–319.
23. Kuai R, Li D, Chen YE, Moon JJ, Schwendeman A. High-density lipoproteins: nature's multifunctional nanoparticles. *ACS Nano*. 2016;10(3):3015–3041.
24. Cruz PM, Mo H, McConathy WJ, Sabnis N, Lacko AG. The role of cholesterol metabolism and cholesterol transport in carcinogenesis: a review of scientific findings, relevant to future cancer therapeutics. *Front Pharmacol*. 2013;4:1–7.
25. Gospodarowicz D, Lui GM, Gonzalez R. High-density lipoproteins and the proliferation of human tumor cells maintained on extracellular matrix-coated dishes and exposed to defined medium. *Cancer Res*. 1982;42(9):3704–3713.
26. Danilo C, Guiterrez-Pajares J, Maineri M, et al. Scavenger receptor class B type 1 regulates cellular cholesterol metabolism and cell signaling associated with breast cancer development. *Breast Cancer Res*. 2013;15(5):R87.
27. Wadsack C, Hirschmugl B, Hammer A, et al. Scavenger receptor class B, type I on non-malignant and malignant human epithelial cells mediates cholesteryl ester-uptake from high density lipoproteins. *Int J Biochem Cell Biol*. 2003;35(4):441–454.
28. Lacko AG, Nair M, Paranjape S, Johnson S, McConathy WJ. High density lipoprotein complexes as delivery vehicles for anticancer drugs. *Anticancer Res*. 2002;22(4):2045–2049.
29. Yuan B, Wu C, Wang X, et al. High scavenger receptor class B type 1 expression is related to tumor aggressiveness and poor prognosis in breast cancer. *Tumor Biol*. 2015;37(3):1–8.
30. Mooberry LK, Nair M, Paranjape S, McConathy WJ, Lacko AG. Receptor mediated uptake of paclitaxel from a synthetic high density lipoprotein nanocarrier. *J Drug Target*. 2010;18(1):53–58.
31. Jiang W, Kim B, Rutka J, Chan W. Nanoparticle-mediated cellular response is size dependent. *Nat Nanotechnol*. 2008;3(3):145–150.
32. National Cancer Institute [webpage on the Internet]. *SEER Fact Sheet: Female Breast Cancer*. 2013. Available from: www.seer.cancer.gov/statfacts/html/breast.html. Accessed April 3, 2016.
33. Dietze EC, Sistrunk C, Miranda-Carboni G, O'Regan R, Seewaldt VL. Triple-negative breast cancer in African-American women: disparities versus biology. *Nat Rev Cancer*. 2015;15(4):248–254.
34. Wabha HA and El-Hadaad HA. Current approaches in treatment of triple-negative breast cancer. *Cancer Biol Med*. 2015;12(2):106-116.
35. Robinson P, Kasembeli M, Bharadwaj U, Engineer N, Eckols KT, Tweardy DJ. Substance P receptor signaling mediates doxorubicin-induced cardiomyocyte apoptosis and triple-negative breast cancer chemoresistance. *Biomed Res Int*. 2016;2016:1959270.
36. Anders CK, Abramson V, Tan T, Dent R. The evolution of triple-negative breast cancer: from biology to novel therapeutics. *Am Soc Clin Oncol Educ Book*. 2016;35:34–42.
37. Zhang Z, Cao W, Jin H, et al. Biomimetic nanocarrier for direct cytosolic drug delivery. *Angew Chem Int Ed Engl*. 2009;48(48):9171–9175.